Adsorption and Dissociation of H_2O_2 on Pt and Pt−Alloy Clusters and Surfaces

Perla B. Balbuena,*,† Sergio R. Calvo,† Eduardo J. Lamas,† Pablo F. Salazar,† and Jorge M. Seminario*,†,‡

Department of Chemical Engineering and Department of Electrical Engineering, Texas A&M University, College Station, Texas 77843

Received: May 17, 2006; In Final Form: July 12, 2006

The adsorption of H_2O_2 on Pt and Pt−M alloys, where M is Cr, Co, or Ni, is investigated using density functional theory. Binding energies calculated with a hybrid DFT functional (B3PW91) are in the range of −0.71 to −0.88 eV for H_2O_2 adsorbed with one of the oxygen atoms on top Pt positions of Pt_3, Pt_2M, and PtM_2, and enhanced values in the range of −0.81 to −1.09 eV are found on top Ni and Co sites of the Pt_2M clusters. Adsorption on top sites of Pt_{10} yields a weaker binding of −0.48 eV, whereas on periodic Pt(111) and Pt_3Co(111) surfaces, H_2O_2 generally dissociates into two OH radicals. On the other hand, attempts to attach H_2O_2 on bridge sites cause spontaneous dissociation of H_2O_2 into two adsorbed OH radicals, suggesting that stable adsorptions on bridge sites are not possible for any of the clusters or extended surfaces that are being studied. We also found that the water−H_2O_2 interaction reduces the strength of the adsorption of H_2O_2 on these clusters and surfaces.

1. Introduction

The oxygen reduction reaction catalyzed by Pt and Pt alloys is extensively investigated because of its importance in several technological and biological processes. The oxygen reduction reaction (ORR) is one of the surface electrode reactions of low-temperature fuel cells, characterized by its slow kinetics even when it takes place on Pt, the best catalyst currently known for this reaction.[1] Improving the performance of such catalytic processes may significantly contribute to enhanced fuel cell performance, which is strongly needed to make fuel cells a commercial reality.[2] Thus, achieving such a goal involves, as a first step, development of a thorough understanding of the ORR mechanism, which is still debated despite vast research efforts.[3−5]

As a summary of the generally accepted knowledge, the oxygen reduction reaction on Pt surfaces in acidic media may proceed via a direct four-electron pathway that reduces O_2 to H_2O by a sequence of four electron and proton transfers, or via a series pathway where H_2O_2 is produced as an intermediate, which is then reduced to water.[3] Recently, we have reported ab initio molecular dynamics[6] and density functional theory[7] data which suggest that a parallel, direct, and series mechanism may be in place under the fuel cell operational conditions, with a dominant direct pathway. Proton exchange fuel cells, currently the most successful low-temperature fuel cells, use a polymer membrane as an electrolyte, which connects the two electrodes, facilitating proton transport from the anode, where a fuel such as H_2 is oxidized, to the cathode where O_2 is reduced.[2,8] In such an environment, the production of H_2O_2 is highly undesired because of its potential for generating radicals that degrade the polymer membrane,[9] one of the most expensive materials of the fuel cell, along with the catalyst. Such proposed membrane degradation mechanisms are based on the decomposition of H_2O_2 into $^{\bullet}OH$ or $^{\bullet}OOH$ radicals, which may attack any H-containing terminal bonds present in the polymer.[8]

To reduce the costs of the catalyst, alternative materials such as Pt alloys have been proposed and extensively tested.[10] Some combinations such as Pt−Co, Pt−Ni, Pt−Cr, Pt−Fe, and other alloys have been found to catalyze the oxygen reduction reaction at least as well as pure Pt.[11−13] However, the presence of a foreign element may favor the production of H_2O_2 with the consequent potential of polymer membrane degradation.[8] Therefore, it is important to identify the conditions under which H_2O_2 may be adsorbed or may generate undesired radical species that could migrate to the membrane.

The catalysts used in current fuel cell technology are Pt-based nanoparticles on the order of 2−10 nm, deposited on activated carbon and surrounded by a hydrated polymer electrolyte membrane.[10] Under such conditions, the metal nanoparticle may have small portions of exposed smooth surfaces but also large amounts of edges, corners, and defects, as a result of the surface dynamics and interactions with the environment (hydrated membrane, reactants, and products). Our study involves the characterization of adsorption of H_2O_2 obtained from density functional theory calculations on three-atom clusters, followed by similar calculations of adsorption on a Pt_{10} cluster and on periodic Pt(111) and Pt_3Co(111) surfaces. The local solvent effect is modeled by adding a few water molecules in the vicinity of the H_2O_2 molecule.

2. Computational Methods

2.1. Clusters. Density functional theory (DFT) as implemented in Gaussian 98[14] is used to calculate the optimized structures, binding energies, Mulliken charge distribution, and vibrational frequencies of Pt and Pt alloy clusters and their interactions with H_2O_2. All calculations were performed using the B3PW91 hybrid functional, which uses a combination of B3[15] exchange functionals and PW91[16,17] correlation functionals. This functional is used in combination with the quasi-relativistic pseudopotential and basis set LANL2DZ (Los Alamos National Laboratory),[18−20] which describes the 1s to 4f core electrons for Pt, Ni, Co, and Cr using effective core pseudopotentials and a basis set specially designed for Pt, Ni, Co, and Cr, and the

* To whom correspondence should be addressed. E-mail: balbuena@tamu.edu and seminario@tamu.edu.
† Department of Chemical Engineering.
‡ Department of Electrical Engineering.

10.1021/jp063027z CCC: $33.50
Published on Web 08/15/2006

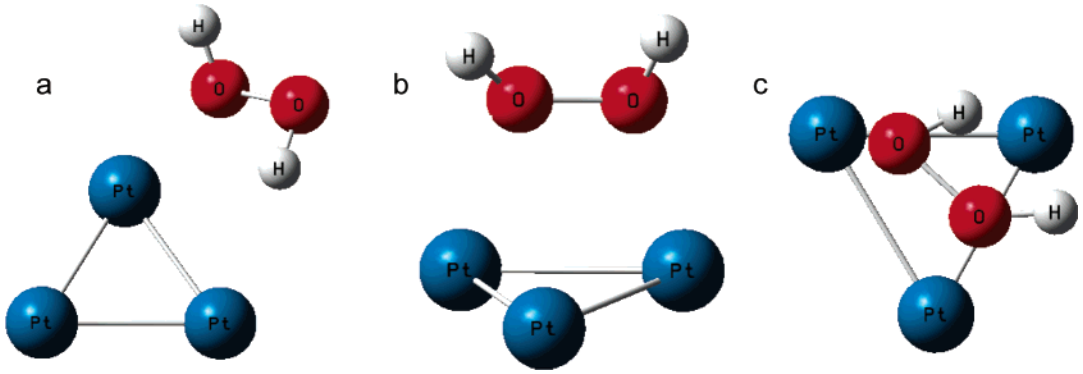

Figure 1. Initial configurations for optimizations of H_2O_2 adsorption on Pt_3, Pt_2M, and PtM_2: (a) top, (b) bridge, and (c) hollow.

TABLE 1: Interatomic Distances, Mulliken Charges, and Total Energies for X−Y−Z Metallic Clusters Obtained with DFT B3PW91/LANL2DZ[a]

X−Y−Z	d_{XY} (Å)	d_{YZ} (Å)	d_{ZX} (Å)	q_X (e)	q_Y (e)	q_Z (e)	m^b	total energy (hartree)
Pt−Pt−Pt	**2.477**	**2.559**	**2.558**	**−0.01**	**−0.01**	**0.02**	**3**	**−357.56024**
Pt−Pt−Pt	2.479	2.48	2.736	−0.01	0.01	0.00	5	−357.52952
Pt−Pt−Ni	**2.565**	**2.389**	**2.389**	**−0.28**	**−0.28**	**0.57**	**3**	**−407.71991**
Pt−Pt−Ni	2.646	2.382	2.382	−0.33	−0.33	0.65	5	−407.69015
Pt−Pt−Co	2.51	2.457	2.455	−0.25	−0.25	0.49	2	−383.47724
Pt−Pt−Co	**2.573**	**2.384**	**2.386**	**−0.28**	**−0.28**	**0.57**	**4**	**−383.48898**
Pt−Pt−Cr	2.587	2.394	2.399	−0.34	−0.34	0.68	6	−383.46917
Pt−Pt−Cr	**2.532**	**2.453**	**2.455**	**−0.33**	**−0.33**	**0.67**	**5**	**−324.73580**
Pt−Ni−Ni	2.5	2.62	2.617	−0.32	−0.32	0.65	7	−324.71876
Pt−Ni−Ni	**2.4**	**2.44**	**2.393**	**−0.45**	**0.22**	**0.23**	**3**	**−457.85610**
Pt−Co−Co	2.393	2.282	2.393	−0.53	0.27	0.26	5	−409.35746
Pt−Co−Co	**2.444**	**2.491**	**2.397**	**−0.41**	**0.23**	**0.18**	**5**	**−409.38345**
Pt−Co−Co	2.397	2.37	2.423	−0.50	0.25	0.25	7	−409.37724
Pt−Ce−Cr	**2.832**	**2.699**	**2.421**	**−0.62**	**0.15**	**0.47**	**3**	**−291.83911**

[a] The optimized geometries show no imaginary frequencies. Several spin states were tested, but only those that differ by less than 1 eV from the ground state (boldface) are included. [b] *m* is the spin multiplicity.

unpolarized double-ξ type for first- and second-row atoms. For hydrogen and oxygen atoms, we use the polarized 6-31G(d) basis set; this combination of functionals, pseudopotentials, and basis sets used to describe the metal−H_2O_2 complexes in this study has proven to be successful in several related applications.[21−23] Following the geometry optimization of all complexes, a second-derivative calculation of the energy with respect to the Cartesian coordinates is performed to confirm the existence of a local minimum and to estimate zero-point energies. The self-consistency of the noninteractive wave function is performed with a convergence threshold for the maximal density matrix of 10^{-8} and 10^{-6} for its rms. These settings provide correct energies of at least five decimal places and geometries of approximately three decimal places within the level of theory.

2.2. Extended Surfaces. DFT calculations using the PBE[24] exchange-correlation functional are performed to analyze H_2O_2 adsorption and dissociation energy on the Pt(111) and Pt_3Co-(111) surfaces using the ab initio plane wave-based program *pwscf* from the quantum ESPRESSO package.[25] The unit cell of Pt and Pt−Co surfaces is modeled as a three-layer slab with four atoms per layer. Periodic boundary conditions are applied in the three spatial dimensions with 10 Å of vacuum space left between periodic images in the *z*-direction, perpendicular to the surface. In all the calculations presented here, the surface geometry is kept constrained. We adapted Vanderbilt ultrasoft pseudopotentials[26] to minimize the computational requirements associated with the description of inert core electrons. The plane wave cutoff energy is set to 100 hartree, and the first Brillouin zone is sampled with a Monkhorst Pack mesh[27] with 7K × 7K × 1K points. To facilitate convergence, fractional occupancies are allowed using the Marzari−Vanderbilt cold smearing scheme[28] within a range of 0.034 eV. To make a fair comparison of the binding energies of H_2O_2 on small clusters and periodic surfaces, we have also calculated adsorption on the same geometries for small clusters using the PBE/PBE exchange correlation functional.

3. Results and Discussion

Initial sites for the geometry optimizations of H_2O_2 interacting with the three-metal atom clusters are top, bridge, and hollow as shown in Figure 1. H_2O_2 adsorbs at the top site when the molecule is initially placed there, but in a few cases, H_2O_2 originally located on a bridge site moves to a top site upon geometry optimization.

3.1. Pt_3, Pt_2M, and PtM_2 Clusters (where M is Ni, Co, or Cr). Table 1 lists the interatomic distances, Mulliken charges, and multiplicities of the ground and higher-energy states of the metal clusters. In all cases, Pt atoms are negatively charged while the different alloying elements (Ni, Co, and Cr) are positively charged. That is evidence of the electron donor capacity of these metal atoms. For Pt_3 and Pt_2M, the clusters arrange as isosceles triangles. In Pt_2M, vertex position Z is occupied by foreign element M, which acts as an electron donor and becomes positive, and the XZ═YZ bond length becomes shorter than those in Pt_3. The PtM_2 clusters arrange as scalene triangles with charge transfer from both M elements to the Pt atom, and the charge on Pt becomes 1.5−2 times higher than that of the Pt atoms in Pt_2M.

Cr is a better electron donor than Ni or Co, and in Pt_2Cr, it is charged with 0.67 e, yielding the highest dipole moment, 4.11 D, found in this set of clusters. This result is in line with the slightly larger difference between the electronegativities of Pt

TABLE 2: Initial and Final Conformations, Binding Energies, and Mulliken Populations of Bimetallic Clusters with a H_2O_2 Ligand, Calculated with DFT (B3PW91 and LANL2Z for the metal elements and 6-31G* for H and O)[a]

system	*m*	initial conformation	final conformation	energy (hartree)	binding energy (eV)	q_Y (e)	q_Z (e)	q_{OM} (e)	q_O (e)	q_{HM} (e)	q_H (e)	structure
$Pt_3-H_2O_2$	1	bridge Pt−Pt (parallel)	atop Pt	−509.06494	−0.78	−0.03	−0.08	−0.45	−0.38	0.51	0.46	A1
$Pt_3-H_2O_2$	1	atop Pt	atop Pt	−509.06358	−0.75	−0.06	−0.08	−0.40	−0.40	0.49	0.50	A2
$Pt_3-H_2O_2$	3	bridge Pt−Pt (perpendicular)	atop Pt	−509.06710	−0.84	−0.08	−0.07	−0.42	−0.39	0.51	0.48	A3
$Pt_3-H_2O_2$	1	atop Pt	atop Pt	−509.06832	−0.88	−0.06	−0.03	−0.42	−0.39	0.50	0.49	A4
$Pt_2Ni-H_2O_2$	3	bridge Pt−Pt (parallel)	dissociation into 2OH	−559.31501	−2.81	−0.01	0.64	−0.74	−0.74	0.44	0.44	B1
$Pt_2Ni-H_2O_3$	5	bridge Pt−Ni (parallel)	dissociation into 2OH	−559.33033	−3.02	−0.25	0.86	−0.64	−0.84	0.50	0.44	B2
$Pt_2Ni-H_2O_2$	3	atop Ni	atop Ni	−559.23491	−1.06	−0.27	0.53	−0.41	−0.45	0.52	0.50	B3
$Pt_2Ni-H_2O_2$	3	bridge Pt−Pt (perpendicular)	atop Ni	−559.23479	−1.06	−0.28	0.53	−0.45	−0.41	0.50	0.52	B4
$Pt_2Ni-H_2O_2$	3	atop Pt	atop Pt	−559.22330	−0.75	−0.35	0.54	−0.42	−0.40	0.49	0.48	B5
$Pt_2Co-H_2O_2$	4	bridge Pt−Pt (parallel)	dissociation into 2OH	−535.08572	−2.83	−0.02	0.65	−0.75	−0.75	0.44	0.44	C1
$Pt_2Co-H_2O_3$	6	bridge Pt−Co (parallel)	dissociation into 2OH	−535.11026	−3.17	0.87	−0.22	−0.73	−0.82	0.45	0.43	C2
$Pt_2Co-H_2O_2$	4	atop Co	atop Co	−535.00493	−1.09	−0.26	0.57	−0.46	−0.41	0.49	0.51	C3
$Pt_2Co-H_2O_2$	4	bridge Pt−Pt (perpendicular)	atop Co	−534.99855	−0.92	−0.33	0.54	−0.41	−0.40	0.49	0.48	C4
$Pt_2Co-H_2O_2$	4	atop Pt	atop Pt	−534.99581	−0.84	−0.33	0.54	−0.41	−0.40	0.49	0.48	C5
$Pt_2Cr-H_2O_2$	5	bridge Pt−Pt (parallel)	dissociation into 2OH	−476.33013	−2.80	−0.08	0.77	−0.75	−0.75	0.44	0.44	D1
$Pt_2Cr-H_2O_2$	3	bridge Pt−Cr (parallel)	dissociation into 2OH	−476.36330	−3.25	−0.26	0.92	−0.77	−0.73	0.45	0.44	D2
$Pt_2Cr-H_2O_2$	3	bridge Pt−Pt (perpendicular)	dissociation into 2OH	−476.37011	−3.34	−0.19	1.05	−0.72	−0.72	0.46	0.46	D3
$Pt_2Cr-H_2O_2$	5	atop Pt	atop Pt	−476.23775	−0.71	−0.38	0.64	−0.41	−0.41	0.49	0.48	D4
$PtNi_2-H_2O_2$	5	bridge Ni−Ni (parallel)	dissociation into 2OH	−609.48936	−3.33	0.62	0.64	−0.83	−0.79	0.43	0.47	E1
$PtNi_2-H_2O_2$	3	atop Ni	atop Ni	−609.36613	−0.93	0.25	0.22	−0.44	−0.42	0.48	0.51	E2
$PtNi_2-H_2O_2$	5	bridge Pt−Ni (parallel)	dissociation into 2OH	−609.46195	−2.96	0.35	0.55	−0.72	−0.81	0.44	0.43	E3
$PtNi_2-H_2O_2$	3	hollow	dissociation into 2OH	−609.49205	−3.37	0.40	0.42	−0.82	−0.75	0.43	0.47	E4
$PtNi_2-H_2O_2$	3	atop Pt	atop Pt	−609.35328	−0.58	0.21	0.17	−0.41	−0.40	0.49	0.48	E5
$PtCo_2-H_2O_2$	5	bridge Co−Co (parallel)	dissociation into 2OH	−561.03377	−3.56	0.75	0.51	−0.82	−0.83	0.42	0.45	F1
$PtCo_2-H_2O_2$	5	atop Co	atop Co	−560.88903	−0.81	0.16	0.13	−0.46	−0.39	0.49	0.44	F2
$PtCo_2-H_2O_2$	7	bridge Pt−Co (parallel)	dissociation into 2OH	−561.03959	−3.64	0.44	0.56	−0.74	−0.83	0.44	0.44	F3
$PtCo_2-H_2O_2$	7	hollow	dissociation into 2OH	−561.03926	−3.64	0.42	0.58	−0.74	−0.83	0.44	0.44	F4
$PtCo_2-H_2O_2$	5	atop Pt	atop Pt	−560.88226	−0.62	0.12	0.19	−0.41	−0.40	0.50	0.48	F5
$PtCr_2-H_2O_2$	3	bridge Cr−Cr (parallel)	dissociation into 2OH	−443.49341	−3.62	0.42	0.72	−0.83	−0.75	0.41	0.47	G1
$PtCr_2-H_2O_2$	3	atop Cr	dissociation into 2OH	−443.50014	−3.71	0.54	0.70	−0.73	−0.88	0.51	0.42	G2
$PtCr_2-H_2O_4$	5	bridge Pt−Co (parallel)	dissociation into 2OH	−443.47363	−3.35	0.17	1.03	−0.75	−0.75	0.45	0.45	G3
$PtCr_2-H_2O_2$	3	hollow	dissociation into 2OH	−443.51656	−3.93	0.68	0.54	−0.78	−0.87	0.43	0.44	G4
$PtCr_2-H_2O_2$	3	atop Pt	atop Pt	−443.32627	−0.31	0.08	0.39	−0.37	−0.41	0.47	0.47	G5
$PtCr_2-H_2O_2$	1	atop Cr	dissociation into 2OH	−443.37668	−2.03	0.41	0.48	−0.78	−0.72	0.44	0.47	G6

[a] For the cases where H_2O_2 is dissociated, the binding energy per adsorbed OH radical is calculated as [energy of the cluster−$(OH)_2$ − energy of cluster − energy of H_2O_2]/2. Structures provided as Supporting Information.

and Cr compared with the other possible interactions (Pt−Pt, Pt−Ni, and Pt−Co). For the Pt−Cr_2 alloy, Cr atoms are charged by 0.15e and 0.47e while the Pt atom bears −0.62e, yielding a net dipole moment of 2.74 D.

3.2. Interaction of H_2O_2 with the Metal Clusters. H_2O_2 is a singlet in its ground state, with calculated bond lengths of 1.44 Å for the O−O bond and 0.97 Å for the O−H bond, a H−O−O angle of 100°, and a dihedral H−O−O−H angle of 117.3°. Its DFT calculated total energy (*E*) is −151.47592 hartree with a dipole moment of 1.84 D. Table 2 lists the initial and final configurations, binding energies, Mulliken populations, and multiplicities of the metal clusters complexed with H_2O_2. It is found that H_2O_2 adsorbs weakly in all clusters but can dissociate spontaneously on the Pt_2M clusters, although the final state depends on the initial location of H_2O_2 with respect to the cluster. Our previous studies indicated that the transition state for dissociation of H_2O_2 from Pt_3 is a bridge configuration.[7] Following the O−O reaction coordinate, we reported the potential energy surface for dissociation of H_2O_2 from Pt_3 yielding an activation energy of 0.57 eV (Figures 2 and 3 in

TABLE 3: Binding Energies (electronvolts) per Adsorbed OH Radical after Spontaneous Dissociation of H_2O_2 Calculated Using B3PW91 with LANL2DZ for Transition Metal Atoms and 6-31G* for H and O Atoms[a]

system	binding energy per OH[b]	adsorption sites	structure	energy of binding of one OH radical to individual sites	binding energy with reference to H_2O_2[c]
$Pt_2Ni-(OH)_2$	−2.81	Pt, Pt	B1	−3.13 (Pt)	−3.24
$Pt_2Ni-(OH)_2$	−3.02	Pt, Ni	B2	−3.13 (Pt), −3.07 (Ni)	−3.66
$Pt_2Co-(OH)_2$	−2.83	Pt, Pt	C1	−2.94 (Pt)	−3.28
$Pt_2Co-(OH)_2$	−3.16	Pt, Co	C2	−2.94 (Pt), −3.56 (Co)	−3.95 **(−1.76)**
$Pt_2Cr-(OH)_2$	−2.80	Pt, Pt	D1	−3.32 (Pt)	−3.22
$Pt_2Cr-(OH)_2$	−3.25	Pt, Cr	D2	−3.58 (Cr)	−4.12
$Pt_2Cr-(OH)_2$	−3.34	Cr (single site)	D3	−3.58 (Cr)	−4.31
$PtNi_2-(OH)_2$	−3.33	Ni, Ni	E1	−3.07 (Ni)	−4.28
$PtNi_2-(OH)_2$	−2.95	Ni, Pt	E3	−3.07 (Ni) −2.74 (Pt)	−3.53
$PtNi_2-(OH)_2$	−3.36	Ni−Pt, Ni−Ni	E4	−3.88 (Ni−Ni)	−4.35
$PtCo_2-(OH)_2$	−3.56	Co, Co−Co	F1	−4.32 (Co−Co)	−4.74 **(−2.24)**
$PtCo_2-(OH)_2$	−3.64, −3.63	Pt−Co, Co−Co	F3, F4	−4.32 (Co−Co)	−4.90
$PtCr_2-(OH)_2$	−3.61	Cr, Cr	G1		−4.85
$PtCr_2-(OH)_2$	−3.71	Cr, Cr	G2		−5.04
$PtCr_2-(OH)_2$	−3.34	Cr (single site)	G3		−4.31
$PtCr_2-(OH)_2$	−3.93	Pt−Cr, Cr−Cr	G4	−4.89 (Cr−Cr)	−5.48
$PtCr_2-(OH)_2$	−2.02	Cr, Cr	G6		−1.68

[a] Values in parentheses in the last column correspond to those calculated using the PBEPBE exchange correlation functional. Structures provided as Supporting Information. [b] Calculated as [energy of cluster−$(OH)_2$ − energy of cluster − 2 × energy of OH]/2. [c] Calculated as [energy of cluster/$(OH)_2$ − energy of cluster − energy of H_2O_2]/2.

ref 5). In the transition state, the O−O bond length is stretched to 1.7 Å, and we note that the dissociation is driven by the strong adsorption of the OH radical.[7] Similarly, in all Pt_2M clusters, when H_2O_2 is initially located on a bridge Pt−Pt site, with the O−O bond parallel to the Pt−Pt bond, the molecule spontaneously dissociates into two OH radicals, each of them adsorbs on one of the Pt atoms, and the adsorption energies are very similar, corresponding to noninteracting adsorbed OH radicals (B1, C1, and D1 in the Supporting Information figure).

When H_2O_2 is located close to one of the PtM bridge sites of Pt_2M, it is also dissociated, resulting in an adsorbed OH radical on top of the Pt and M sites. The adsorption energy of the OH radicals interacting with M and Pt (B2, C2, and D2 in the Supporting Information figure) is slightly enhanced with respect to those in which the two OH radicals are adsorbed on Pt atoms (B1, C1, and D1). In Pt_2Cr, the dissociation is easier, and from various initial sites (Table 2 and Supporting Information figure), including dissociation by a single Cr atom (D3) where the two OH radicals are adsorbed. The exception is when H_2O_2 is initially placed with one of the O atoms on top of a Pt atom of Pt_2Cr, where a relatively weak adsorption is obtained (binding energy of −0.71 eV). Such a weak adsorption state is also found in Pt_3 (0.75−0.88 eV in A1−A4) and in the other Pt_2M clusters as well, although the adsorption strength is higher on top of Co (C3) and Ni atoms (B3 and B4).

The tendency of H_2O_2 to dissociate is enhanced when it interacts with the PtM_2 clusters; initial configurations that favor dissociation include H_2O_2 located on a Pt−M bridge, with the O−O bond parallel to the Pt−M bond, and a "hollow" location where the molecule is located above the hollow site, one of the O atoms interacting with one metal atom and the H atom of the opposite side interacting with another metal atom. Initial adsorbate locations on top of the Pt atom yield adsorption states (E5, F5, and G5) even weaker than those of Pt_3 (A1−A4) and Pt_2M (B5, C5, and D4), but slightly higher adsorptions are found on top of Ni (E2) and Co (F2).

In the $Pt_3-H_2O_2$ complex (structure A4), the H atoms have Mulliken charges of 0.50e and 0.49e while oxygen atoms have charges of −0.42e and −0.39e. Thus, the net charge transfer from H_2O_2 to the cluster is 0.18e, leading to a net dipole moment of 1.74 D (0.69 au) for the complex. In general, for all cases in which H_2O_2 is adsorbed at top site positions, we find a net charge transfer from H_2O_2 to the cluster which becomes slightly negatively charged. The O−O distances in adsorbed H_2O_2 ranging from 1.449 Å (C4) to 1.474 Å (B5) are slightly longer than the distance of 1.441 Å obtained for free H_2O_2 in the gas phase, with red-shifted frequencies compared with that of free H_2O_2 (943.5 cm^{-1}).

We have computed the energy differences between ground and higher-energy (metastable) states for each complex; this material is available as Supporting Information. With a few exceptions found especially in the $PtM_2-H_2O_2$ complexes, the differences between ground and metastable states are minimal.

Upon H_2O_2 dissociation, OH radicals are strongly adsorbed on top sites. The weakest adsorption corresponds to the Pt−$(Cr-OH)_2$ complex, structure G6, with a binding energy of −2.03 eV per OH radical. The binding energies reported in Table 2 and the Supporting Information figure were calculated by taking the metal cluster and free H_2O_2 as reference states. In Table 3, we also take the metal cluster and two OH radicals as reference states and compare the binding energies with those previously reported for adsorption of single-OH species on the same clusters.[22] Table 3 shows that the binding energy per OH radical obtained for the simultaneous adsorption of two OH radicals is only slightly less exothermic than that for a single OH radical in the same clusters, suggesting a small degree of interaction between the two adsorbed OH species. Dissociation of H_2O_2 from $PtCr_2$ can result in adsorption of one OH radical to each of the two Cr atoms in $PtCr_2$ (G1, G2, and G6). Comparison of structures G1 and G2 with G6 indicates that although the O−Cr distances are very similar, the Cr−Cr distance in G6 is much shorter (∼1 Å) than in G1 and G2, which may cause repulsion between the adsorbed radicals, decreasing their binding energy. In all the dissociation cases, we found a negative charge transfer from the cluster to the OH radical, approximately −0.30e per OH. This charge is compensated by the positive net charge of the cluster, reflecting its electron donor capacity.

3.3. Effect of Cluster Size. We evaluate how the H_2O_2 binding energy changes with the metal cluster size using a Pt_{10} cluster with a fixed geometry (Figure 2). The spin multiplicity ($m = 9$) corresponding to the minimum energy was determined

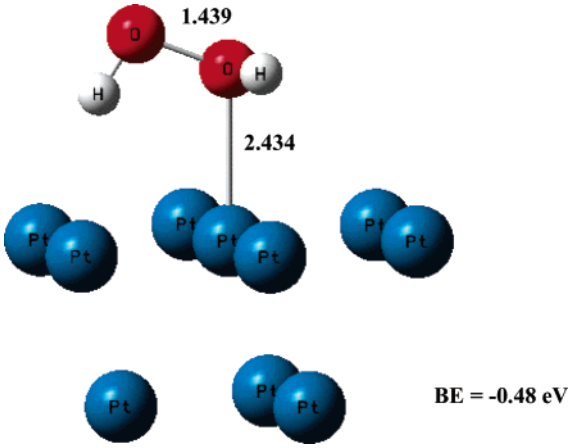

Figure 2. Optimized structure and binding energy for the $Pt_{10}-H_2O_2$ complex.

by self-consistent field calculations of Pt_{10} clusters with multiplicities of 1, 3, 5, 7, 9, and 11. The binding energy of H_2O_2 on top sites is −0.48 eV, much weaker than that on Pt_3 (−0.75 eV), which is reflected on an elongated Pt−O distance for the $Pt_{10}-H_2O_2$ complex of 2.43 Å, 0.2 Å longer than that in Pt_3· H_2O_2 also dissociates from Pt_{10} when the molecule is initially located close to its bridge site transition state geometry. These results are in agreement with those in previous work[7] where we also reported the existence of weak H_2O_2-adsorbed states in Pt_3, Pt_4, Pt_6, and Pt_{10}; their binding energies computed at the B3LYP/6-311++G** level are comparable with our current values and also showed a slight decrease in the adsorption strength as the number of metal atoms in the cluster increases.

3.4. Adsorption of H_2O_2 on Extended Pt(111) and Pt_3Co-(111) Surfaces. Figure 3 illustrates the initial configurations of H_2O_2 on the bridge position of Pt(111) and on the top position of $Pt_3Co(111)$. Calculations on extended surfaces include Pt-(111) and two Pt skin systems of $Pt_3Co(111)$ with different underlying Co distributions: one with zero, two, and one Co atom in the first, second, and third layers, respectively, of the metal slab and the other with zero, one, and two Co atoms, respectively (Figure 3). To establish a reference, optimizations of a clean slab and of a single H_2O_2 molecule are performed. The ground state electronic configuration for H_2O_2 is found to be a singlet with O−O and O−H bond lengths of 1.47 and 0.98 Å, respectively, an O−H−H angle of 100°, and a dihedral H−O−O−H angle of 112°. When it is placed over the surface on bridge or top locations with a closest distance of ∼2 Å (Figure 3b), dissociation was observed in all cases (Figure 4a), with dissociation energies shown in Table 4. However, when it is placed at a distance greater than 2.6 Å (geometry as shown

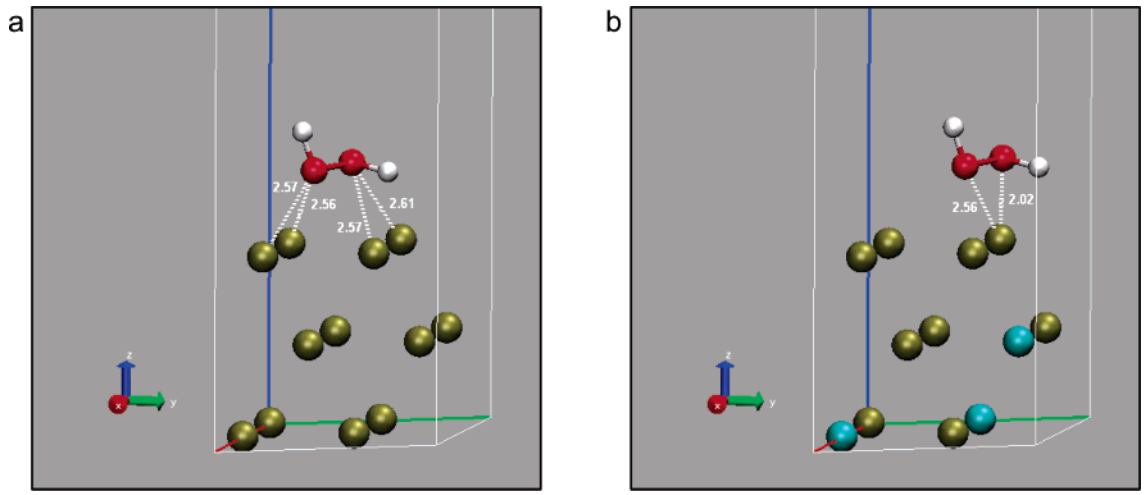

Figure 3. Initial configurations of H_2O_2 on (a) the bridge site of Pt(111) and (b) the top site of $Pt_3Co(111)$. Pt atoms are colored gold and Co atoms blue.

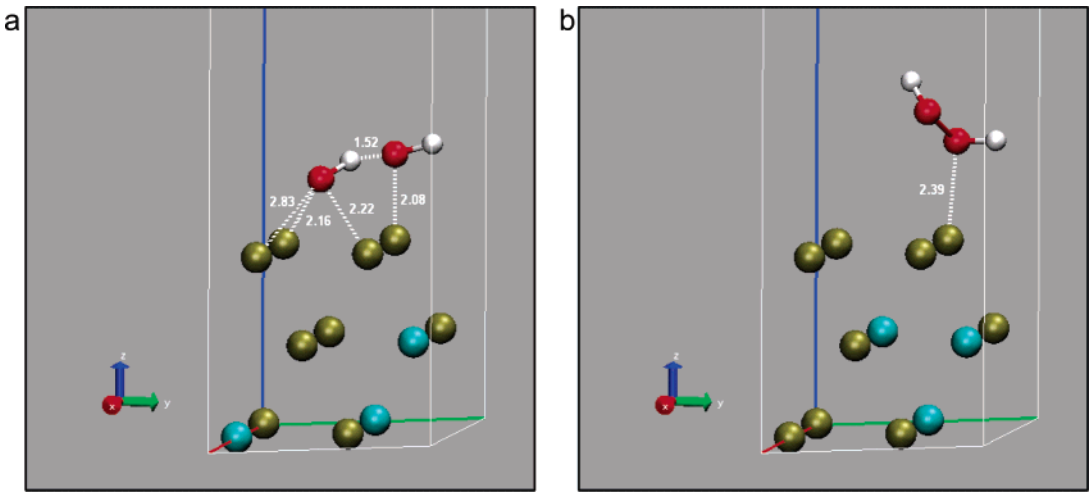

Figure 4. Final configurations of H_2O_2: (a) dissociated, one OH radical adsorbed on the bridge site and the other on top of a Pt skin configuration of $Pt_3Co(111)$; and (b) weakly adsorbed on top of a Pt skin configuration of $Pt_3Co(111)$. Pt atoms are colored gold and Co atoms blue.

TABLE 4: Binding Energies (in electronvolt) per Adsorbed OH Radical after Spontaneous Dissociation of H_2O_2, Calculated as [energy of slab−$(OH)_2$ − energy of slab − energy of H_2O_2]/2

system	reference states	energy (Ry)	binding energy (eV)
Pt(111)−H_2O_2 bridge−top	Pt(111)	−1065.62427	−0.98
	H_2O_2	−66.26559	
	Pt(111)−H_2O_2	−1132.03378	
Pt(111)−H_2O_2 top−top	Pt(111)	−1065.62427	−1.03
	H_2O_2	−66.26559	
	Pt(111)−H_2O_2	−1132.04094	
Pt_3Co(111)−H_2O_2 bridge−top; Co atomic distribution: 0, 1, 2	Pt_3Co(111)	−1039.63188	−0.93
	H_2O_2	−66.26559	
	Pt(111)−H_2O_2	−1106.03420	
Pt_3Co(111)−H_2O_2 top−top; Co atomic distribution: 0, 2, 1	Pt_3Co(111)	−1039.68704	−0.98
	H_2O_2	−66.26559	
	Pt(111)−H_2O_2	−1106.09640	

in Figure 3a), the molecule adsorbs in a tilted manner without dissociation, with one oxygen atom over a top Pt position of Pt_3Co (Figure 4b), and a very small adsorption energy of −0.03 eV.

Once dissociated, the two OH-adsorbed species arrange on the surface in a configuration that favors hydrogen bonding between OH species in neighbor positions. The adsorption energies given in Table 4 are with reference to H_2O_2 and can be compared with those reported in Table 3 (last column, values in parentheses) for Pt_2Co and $PtCo_2$ calculated with the same PBE/PBE exchange correlation functional. Such a comparison reveals that there is a substantial difference between the binding energies of the adsorbed OH species on the small clusters and on the periodic surfaces; in the small clusters, the binding energy is approximately twice that found in the extended surfaces. Binding energies per OH radical calculated on the extended surfaces as (energy of slab−H_2O_2 − energy of slab − 2 × energy of OH)/2 equal −2.10 and −2.08 eV, respectively, for the two different distributions of subsurface Co in the Pt_3Co(111) slabs. These values are ∼0.1−0.2 eV less than those reported by Panchenko et al. for a one-fourth monolayer OH radical adsorbed on Pt(111).[29]

Table 3 also illustrates the differences between the DFT calculated energy values on the same systems using different functionals. The B3PW91 hybrid yields much higher binding energies: for two OH species adsorbed on Pt_2Co clusters, −3.95 eV versus −1.76 eV obtained with the "pure" PBE/PBE and −4.74 eV versus −2.24 eV for adsorption on $PtCo_2$ clusters. The hybrid functional is known to produce smaller errors than the pure functional for well-tested systems;[30,31] however, extrapolation of such accuracy in nontested systems cannot be assured for the hybrid functional, whereas such extrapolation can be expected to hold for the pure (nonempirical) functional. In summary, independent of the absolute binding energy values, these results definitely suggest well-defined adsorption trends: stronger binding of undissociated H_2O_2 in small clusters than

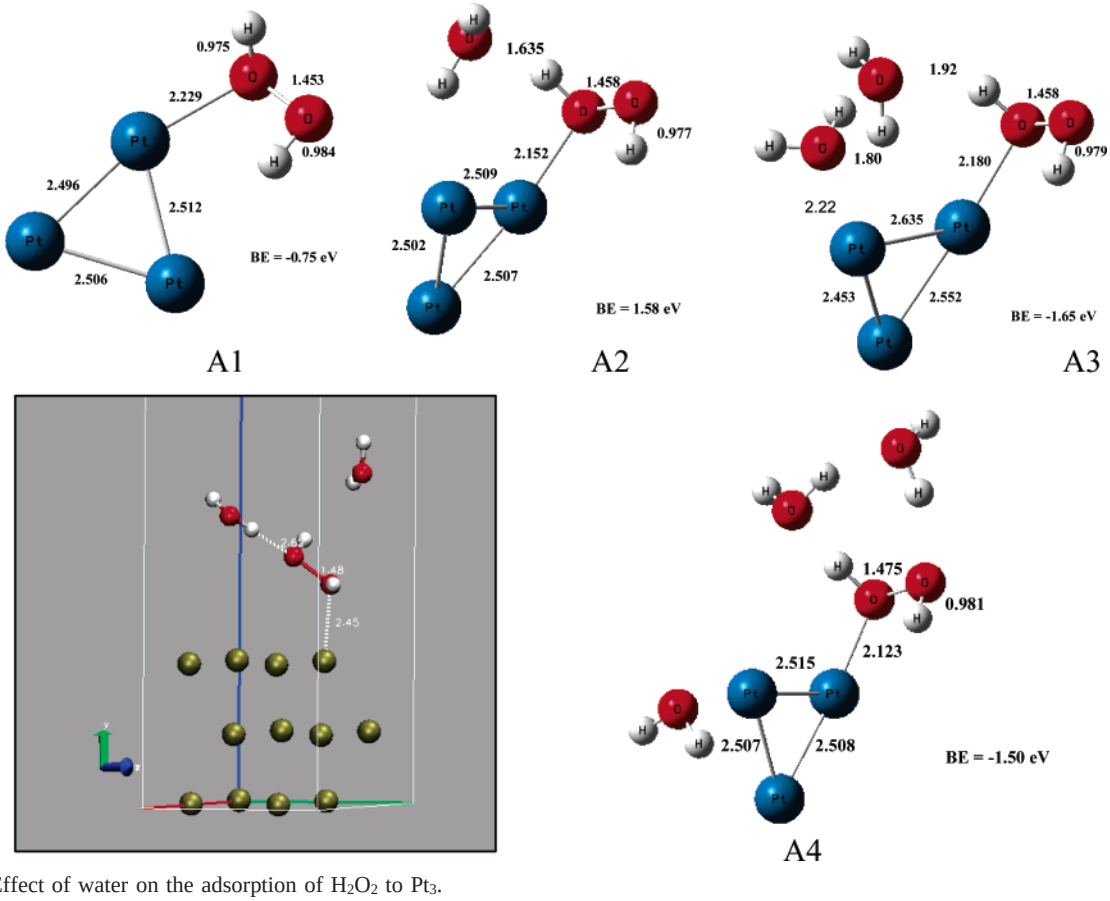

Figure 5. Effect of water on the adsorption of H_2O_2 to Pt_3.

TABLE 5: DFT (B3PW91 with LANL2DZ for transition metals and 6-31G* for H and O)-Calculated Total and Binding Energies for H_2O_2 Solvated by nH_2O (n = 0, 1, 2, and 3) Interacting with Pt_3 As Shown in Figure 5

system	m	E (hartree)	BE (eV)
$Pt_3-H_2O_2$	1	−509.06494	−0.77
$Pt_3-H_2O_2-H_2O$	1	−585.47591	1.58
$Pt_3-H_2O_2-H_2O$	3	−585.47302	1.66
$Pt_3-H_2O_2-2H_2O$	1	−661.88875	−1.50
$Pt_3-H_2O_2-2H_2O$	3	−661.89451	−1.65
$Pt_3-H_2O_2-3H_2O$	3	−738.29257	−1.50

in extended surfaces and spontaneous dissociation of H_2O_2 on bridge sites of small clusters and extended surfaces. It can also be established that sites other than Pt (especially Cr, but also Co and Ni) may be even more favorable for inducing H_2O_2 dissociation.

3.5. Solvent Effect. Binding energies of H_2O_2 in the $Pt_3-H_2O_2-nH_2O$ systems (n = 0, 1, 2, and 3) were calculated to assess the water effect. Analysis of the case in which H_2O_2 is solvated by one water molecule reveals that the presence of water alters the interaction between H_2O_2 and the metal cluster, turning it into a repulsive interaction, as reflected in the binding energy (Table 5) computed as

$$\mathrm{BE} = E_{\mathrm{Pt_3-H_2O_2-}n\mathrm{H_2O}} - E_{\mathrm{H_2O_2-}n\mathrm{H_2O}} - E_{\mathrm{Pt_3}}$$

This repulsive interaction is due to the formation of a strong complex between H_2O_2 and H_2O (binding energy of −3.16 eV) forming a H-bond (O−H distance of 1.635 Å, Figure 5, A2); such a complex weakens the interaction of H_2O_2 with the cluster. As a second water molecule is added to the system (Figure 5, A3), the binding energy becomes attractive (Table 5); this is due to the interaction of the second water with a Pt atom. In addition, the H-bond between H_2O and H_2O_2 becomes weakened (O−H distance of 1.92 Å), and a new H-bond is formed between the two water molecules (O−H distance of 1.80 Å), thus partially restoring the strength of the $H_2O_2-Pt_3$ interaction. Similar conclusions were obtained from analyses of water clusters surrounding sulfonic sites and interacting with the O_2 molecule adsorbed on Pt_3.[32]

A weakened interaction was also obtained from calculations in extended surfaces where one H_2O_2 molecule and two water molecules were included in the unit cell (Figure 5). Moreover, periodic DFT calculations on various slabs of Pt, PtCo, and PdCo where H_2O_2 (surrounded by two water molecules) was initially located on bridge sites indicated that only a Pd surface was able to induce H_2O_2 dissociation. Thus, water may combine with H_2O_2 forming H-bonded complexes, reducing the strength of the interaction of H_2O_2 with the metal atoms. In addition, we did not find spontaneous dissociation when solvated H_2O_2 (with one or two water molecules) is initially located on a bridge site of the metal cluster.

3.6. Effect of the Surrounding Metal Atoms on the Small Clusters. To evaluate the effect of the bulk metal on our cluster results, we tested three cases using a DFT-Green function methodology reported in our previous studies.[21] The idea behind this approach is that in a real system, adsorbates are chemically attached to real catalysts, made of atoms, and not to ideal extended surfaces. Therefore, the interfacial phenomenon is analyzed by coupling matrices obtained at a molecular level from the information about the extended molecule interacting with the active site (i.e., the molecule attached to a few atoms from the catalysts as in the $H_2O_2-Pt_3$ complex) to the results of periodic calculations for the bulk metal, where the active sites are embedded. We claim that our calculations consider explicitly the chemistry of the attachment of the molecule to the catalyst in contrast with simulations of a molecule attached to a perfect or ideal surface.

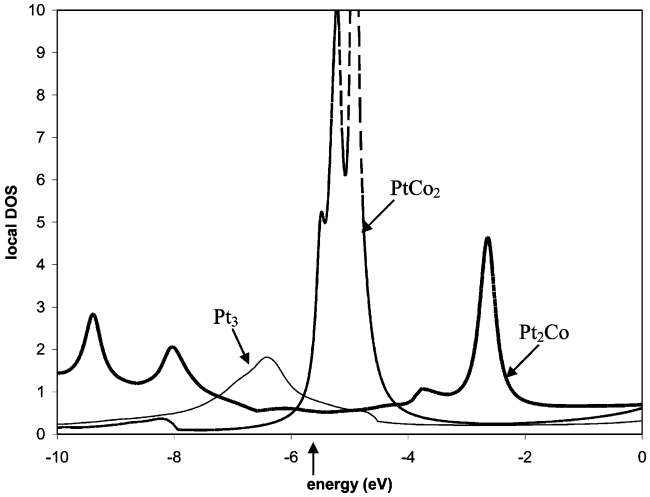

Figure 6. Local density of electronic states (arbitrary units) for the Pt_3, Pt_2Co, and $PtCo_2$ systems, embedded in a Pt continuum metal. Note the effect of the foreign atoms, in particular at the Fermi level of Pt, −5.93 eV.

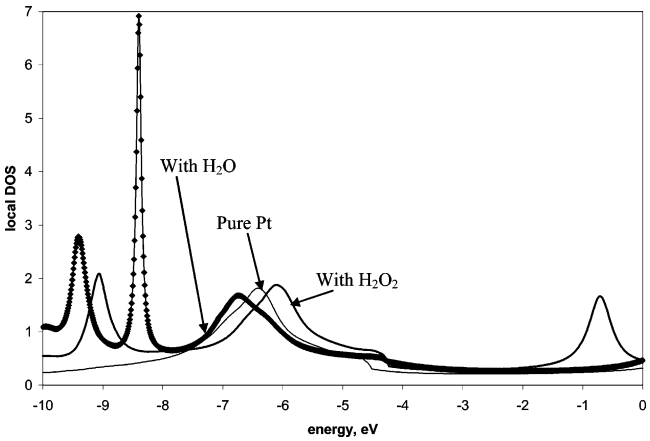

Figure 7. Effect of adsorbates on the local DOS for pure Pt, calculated as Pt_3/adsorbate embedded in bulk Pt.

Figure 6 illustrates the local density of states calculated at the active sites. The peak centered at approximately −6.5 eV corresponds to the Pt d-band, which is located very close to the Pt Fermi level (experimental value of −5.93 eV[33]), whereas in the same neighborhood of the Fermi level, the presence of two Co atoms neighbor to a Pt atom causes a significant increase in the DOS, most likely including occupied and unoccupied states, signaling an enhanced reactivity of the system. A different effect is due to the presence of a single Co atom surrounding two Pt atoms in the active site that shows an enhancement of only the unoccupied states.

The presence of the adsorbate in the DOS of pure Pt is analyzed in Figure 7. With one H_2O_2 molecule adsorbed, there is a shift of the high-density peak toward the Fermi level; the peak shifts left when one water molecule is added (case of A2 in Figure 5), reducing the availability of accessible states at the Fermi level, as suggested by the repulsive energies given by the cluster calculations.

4. Conclusions

Density functional theory studies indicate that H_2O_2 binds weakly on top Pt positions of Pt_3 and Pt_2M and up to 20%

stronger adsorption is found on top sites of Ni and Co of the Pt_2M clusters, whereas when initially placed especially on bridge locations, but also on hollow sites, of Pt_2M and PtM_2, H_2O_2 tends to spontaneously dissociate into two adsorbed OH radicals. Adsorption on top sites of Pt_{10} yields a weaker binding of −0.48 eV, whereas on periodic Pt(111) and $Pt_3Co(111)$ surfaces, H_2O_2 generally dissociates into two OH radicals; however, H_2O_2 binds with an extremely weak adsorption of approximately −0.03 eV on a Pt skin configuration of $Pt_3Co(111)$. Water combines with H_2O_2, forming H-bonded complexes and reducing the strength of the interaction with the metal atoms.

To conclude, it is useful to discuss the relevance of these findings in relation to the oxygen reduction reaction. Let's recall that the production of H_2O_2 during the ORR process is not desired for two reasons: if H_2O_2 dissociates on the electrocatalyst, it produces usually strongly adsorbed OH radicals which occupy sites that would otherwise be available for a further increase in the O_2 reduction current; if H_2O_2 formed during the O_2 reduction process is desorbed from the electrocatalyst and dissociates in the electrolyte phase, yielding $^{\bullet}OH$ or $^{\bullet}OOH$ radicals, these may initiate a degradation reaction involving the polymer membrane as discussed in the Introduction.

Our results indicate stronger binding of undissociated H_2O_2 in small clusters than in extended surfaces and spontaneous dissociation of H_2O_2 on bridge sites of small clusters and extended surfaces, with sites other than Pt (especially Cr, but also Co and Ni) being even more favorable for inducing H_2O_2 dissociation. However, we also find that solvated H_2O_2 may be less prone to becoming adsorbed and/or dissociated. The significant differences detected with respect to the extent of adsorption suggest that active sites such as corners and edges on nanoparticles may play a significant role in the adsorption of undesired intermediate species such as H_2O_2 and its dissociation products. The generation and strong adsorption of OH radicals may be considered a factor that does not support the use of alternative metals such as Co, Cr, or Ni; however, those metals also should be useful in readily dissociating the radical OOH avoiding the initial formation of H_2O_2, which would constitute the best scenario. Therefore, bimetallic or even multimetallic combinations may be very efficiently designed on the basis of the concept that each of the metals would be involved in different reaction steps.[34,35]

Acknowledgment. Financial support from the Department of Energy, Basic Energy Sciences (DE-FG02-05ER15729), is gratefully acknowledged. This research used computational resources of the National Energy Research Scientific Computing Center, which is supported by the Office of Science of the U.S. Department of Energy under Contract DE-AC03-76SF00098, and of the TAMU Supercomputer Center.

Supporting Information Available: Energy differences (in electronvolts) between the ground state and higher-energy states for the systems in Table 2 and optimized structures and binding energies corresponding to Table 2. This material is available free of charge via the Internet at http://pubs.acs.org.

References and Notes

(1) Markovic, N. M.; Ross, P. N. *Surf. Sci. Rep.* **2002**, *45*, 117−229.
(2) Steele, B. C. H.; Heinzel, A. *Nature* **2001**, *414*, 345−352.
(3) Adzic, R. Recent advances in the kinetics of oxygen reduction. In *Electrocatalysis*; Lipkowski, J., Ross, P. N., Eds.; Wiley-VCH: New York, 1998; pp 197−242.
(4) Anderson, A. B.; Albu, T. V. *J. Electrochem. Soc.* **2000**, *147*, 4229−4238.
(5) Anderson, A. B.; Roques, J.; Mukerjee, S.; Murthi, V. S.; Markovic, N. M.; Stamenkovic, V. *J. Phys. Chem. B* **2005**, *109*, 1198−1203.
(6) Wang, Y.; Balbuena, P. B. *J. Phys. Chem. B* **2005**, *109*, 14896−14907.
(7) Wang, Y.; Balbuena, P. B. *J. Chem. Theory Comput.* **2005**, *1*, 935−943.
(8) Curtin, D. E.; Lousenberg, R. D.; Henry, T. J.; Tangeman, P. C.; Tisack, M. E. *J. Power Sources* **2004**, *131*, 41−48.
(9) Pianca, M.; Barchiesi, E.; Esposto, G.; Radice, S. *J. Fluorine Chem.* **1999**, *95*, 71−84.
(10) Gasteiger, H. A.; Kocha, S. S.; Sompalli, B.; Wagner, F. T. *Appl. Catal., B* **2005**, *56*, 9−35.
(11) Paulus, U. A.; Vokaun, A.; Scherer, G. G.; Schmidt, T. J.; Stamenkovic, V.; Radmilovic, V.; Markovic, N. M.; Ross, P. N. *J. Phys. Chem. B* **2002**, *106*, 4181−4191.
(12) Murthi, V. S.; Urian, R. C.; Mukerjee, S. *J. Phys. Chem. B* **2004**, *108*, 11011−11023.
(13) Zhang, J.; Mo, Y.; Vukmirovic, M. B.; Klie, R.; Sasaki, K.; Adzic, R. R. *J. Phys. Chem. B* **2004**, *108*, 10955−10964.
(14) Frisch, M. J.; Trucks, G. W.; Schlegel, H. B.; Scuseria, G. E.; Robb, M. A.; Cheeseman, J. R.; Zakrzewski, V. G.; Montgomery, J. A.; Stratmann, R. E.; Burant, J. C.; Dapprich, S.; Millam, J. M.; Daniels, A. D.; Kudin, K. N.; Strain, O. F. M. C.; Tomasi, J.; Barone, B.; Cossi, M.; Cammi, R.; Mennucci, B.; Pomelli, C.; Adamo, C.; Clifford, S.; Ochterski, J.; Petersson, G. A.; Ayala, P. Y.; Cui, Q.; Morokuma, K.; Malick, D. K.; Rabuck, A. D.; Raghavachari, K.; Foresman, J. B.; Ciolovski, J.; Ortiz, J. V.; Stefanov, V. V.; Liu, G.; Liashensko, A.; Piskorz, P.; Komaroni, I.; Gomperts, R.; Martin, R. L.; Fox, D. J.; Keith, T.; Al-Laham, M. A.; Peng, C. Y.; Nanayakkara, A.; Gonzalez, C.; Challacombe, M.; Gill, P. M. W.; Johnson, B.; Chen, W.; Wong, M. W.; Andres, J. L.; Head-Gordon, M.; Replogle, E. S.; Pople, J. A. *GAUSSIAN 98*, revision A.11; Gaussian Inc.: Pittsburgh, PA, 1998.
(15) Becke, A. D. *J. Chem. Phys.* **1993**, *98*, 1372−1377.
(16) Perdew, J. P.; Chevary, J. A.; Vosko, S. H.; Jackson, K. A.; Pederson, M. R.; Singh, D. J.; Fiolhais, C. *Phys. Rev. B* **1992**, *46*, 6671−6687.
(17) Perdew, J. P.; Wang, Y. *Phys. Rev. B* **1992**, *45*, 13244−13249.
(18) Wadt, W. R.; Hay, P. J. *J. Chem. Phys.* **1985**, *82*, 284−298.
(19) Hay, P. J.; Wadt, W. R. *J. Chem. Phys.* **1985**, *82*, 270−283.
(20) Hay, P. J. *J. Chem. Phys.* **1977**, *66*, 4377.
(21) Balbuena, P. B.; Altomare, D.; Agapito, L. A.; Seminario, J. M. *J. Phys. Chem. B* **2003**, *107*, 13671−13680.
(22) Balbuena, P. B.; Altomare, D.; Vadlamani, N.; Bingi, S.; Agapito, L. A.; Seminario, J. M. *J. Phys. Chem. A* **2004**, *108*, 6378−6384.
(23) Seminario, J. M.; Agapito, L. A.; Yan, L.; Balbuena, P. B. *Chem. Phys. Lett.* **2005**, *410*, 275−281.
(24) Perdew, J. P.; Burke, K.; Ernzerhof, M. *Phys. Rev. Lett.* **1997**, *78*, 1396−1396.
(25) Scandolo, S.; Giannozzi, P.; Cavazzoni, C.; deGironcoli, S.; Pasquarello, A.; Baroni, S. *Z. Kristallogr.* **2005**, *220*, 574−579.
(26) Vanderbilt, D. *Phys. Rev. B* **1990**, *41*, 7892.
(27) Monkhorst, H. J.; Pack, J. D. *Phys. Rev. B* **1976**, *13*, 5188−5192.
(28) Marzari, N.; Vanderbilt, D.; Vita, A. D.; Payne, M. C. *Phys. Rev. Lett.* **1999**, *82*, 3296−3299.
(29) Panchenko, A.; Koper, M. T. M.; Shubina, T. E.; Mitchell, S. J.; Roduner, E. *J. Electrochem. Soc.* **2004**, *151*, A2016−A2027.
(30) Seminario, J. M.; Maffei, M. G.; Agapito, L. A.; Salazar, P. F. *J. Phys. Chem. A* **2006**, *110*, 1060−1064.
(31) Agapito, L. A.; Maffei, M. G.; Salazar, P. F.; Seminario, J. M. *J. Phys. Chem. A* **2006**, *110*, 4260−4265.
(32) Yan, L.; Balbuena, P. B.; Seminario, J. M. *J. Phys. Chem. A* **2006**, *110*, 4574−4581.
(33) *Handbook of Chemistry and Physics*, 77th ed.; Lide, D. R., Ed.; CRC Press: Boca Raton, FL, 1997.
(34) Wang, Y.; Balbuena, P. B. *J. Phys. Chem. B* **2005**, *109*, 18902−18906.
(35) Shao, M. H.; Sasaki, K.; Adzic, R. R. *J. Am. Chem. Soc.* **2006**, *128*, 3526−3527.